Base Plate in Bending and Anchor Bolts in Tension

Wald F., Jaspart J. P., Sokol Z., Brown D.

Summary

The paper describes behaviour of the base plate in bending and the anchor bolts in tension, which is the major component of the base plate connection. The analytical model predicts the component characteristics – the resistance and the stiffness. It is described how the quality of the behaviour is guided by the contact between the base plate and the concrete surface. The presented analytical prediction model is verified on tests and FE simulation.

NOTATION

d	diameter of the bolt
f_y	yield stress of steel
k	component stiffness
m	distance from the bolt axes to the weld edge, bending resistance of base plate
n	distance from the bolt axes to late edge
p	pitch
t	thickness of the base plate
w	bolt pitch
x, y, z	axes
A_s	net area of the bolt
B	bolt force
E	Young's modulus of steel
F	force
L_b	free length of the anchor bolt
Q	prying force
δ	deformation
γ	partial safety factor
κ	coefficient
ℓ	length of the T stub

Subscripts

b	effective free length of bolt
bf	physical free length of bolt
bp	embedded free length of bolt
bp	cover plate
cp	circular pattern
eff	effective
em	embedment
h	bolt head
j	joint

ini	initial
bn	boundary
np	non-circular pattern
p	plate
t	tension
T	T stub
1, 2, 3	mode number

1 Introduction

The base plate connections of the column base have a different configuration compared to the beam to column connections with end plates. The base plates are designed thicker to transfer primarily the compression forces into concrete block and are more stiffened by the stiffeners or by the column. The used anchor bolts are longer compared to the bolts in the end plates due to the presence of the washer plates, the higher thickness of the base plate, the grout, and the embeddement in concrete. The length of the anchor bolts allows deformation and separation of the base plate during the loading of anchor in tension. The difference should be introduced into the prediction of the strength [1], the stiffness and the rotational capacity of the base plate loaded in tension.

The behaviour of the tension part of the base plate is guiding the column base stiffness [2]. Published models of the column base under bending include different levels of modelling of the tension part of the column base from very complex solutions [3] to very simple models [4]. The knowledge of the behaviour of the end plates in the beam to column connections were precised in [4] using knowledge and models developed in the last years [5], [9] by applying the component method [6]. In this method, the connection is disintegrated into components, which behaviour is described, and finally the connection characteristics are composed. The modelling of the column base with the base plate using component method [7] has several advantages, the most important is separate modelling of components.

When the anchor bolts are activated in tension, the base deforms in bending while the anchor bolts elongate [8]. The failure of the tensile zone could be caused by yielding of the plate, failure of the anchor bolts, or combination of both phenomena.

Figure 1 The T stub - anchor bolts in tension and base plate in bending, assumption of the acting forces and deformations

2 Beam model of the T stub

The model of the deformation curve of the T-stub for the initial elastic behaviour may be based on similar assumptions used for modelling of contact of two steel plates [10]. A beam theory, see Figure 1, can be used to derive model of the T-stub loaded by tensile force F. One half of the T-stub is shown on the picture. In case of prying of the anchor bolts, the bolts are loaded by the additional prying force Q, which is balanced by the contact force at the edge of the T-stub. The deformed shape of the curve is described by a differential equation

$$E I \delta'' = -M \tag{1}$$

Figure 2 The beam model of the T-stub

Writing the above equation for the part ・ of the T-stub gives

$$E I \delta_2'' = Q(x - n) \tag{2}$$

and the equation for the part ① close to the centreline of the T-stub is

$$E I \delta_1'' = -\frac{F}{2} x - Q n \tag{3}$$

The equations for the deformed shape of the T-stub are obtained by integrating the equations (2) and (3) and substituting the boundary conditions. The equation for the deflection on the part ① of the T-stub is

$$\delta_1 = \frac{F}{2 E I}\left[\frac{x^3}{3} - \frac{n \kappa}{2}\left(x^2 - 2 m x\right) - \frac{m^2 x}{2} + \frac{L_b I}{A_s}(1 - \kappa)\right] \tag{4}$$

The equation for the deflection of the part ・ of the T-stub is

$$\delta_2 = \frac{F}{2 E I}\left[\frac{\kappa x^3}{3} - \frac{n \kappa}{2}\left(x^2 - 2 m x\right) - \frac{m^2 x}{2} + \frac{L_b I}{A_s}(1 - \kappa)\right] \tag{5}$$

and the coefficient κ is defined

$$\kappa = \frac{3}{2}\left(\frac{2 L_b I - m^2 n A_s}{n^3 A_s + 3 m n^2 A_s + 3 L_b I}\right) \tag{6}$$

In the above equations, the m and n are dimensions of the T-stub defined at the Figure 1 and L_b and A_s are bolt length and the net area of the bolt respectively. The second moment of area of the base plate cross-section is defined as

$$I = \frac{1}{12} \ell_{eff} \, t^3 \tag{7}$$

The boundary for the prying / no prying of the anchor bolts could be obtained from the above equations by setting the prying force equal to zero. When there is no prying force, the contact of the T-stub and the concrete block is interrupted and the previous equations are not valid. The deformation of the bolt and of the base plate are given by the following formulas

$$\delta_b = \frac{F}{2} \frac{L_b}{A_s \, E}, \tag{8}$$

and

$$\delta_p = \frac{F}{2} \frac{m^3}{3 \, E \, I}. \tag{9}$$

The bolt stiffness is defined

$$k_b = \frac{F}{E \, \delta_b} = 2{,}0 \, \frac{A_s}{L_b}, \tag{10}$$

and the plate stiffness of the T stub is

$$k_p = \ell_{eff.ini} \, \beta^3. \tag{11}$$

The total stiffness of both components in case of no contact between the concrete surface and the T-stub is

$$k_{T3} = \frac{F}{E\,(\delta_p + \delta_b)}. \tag{12}$$

which can be rewritten in the component stiffness format

$$k_{T3} = \left(\frac{k_b\ k_p}{k_b + k_p} \right) \tag{13}$$

If the contact between the T-stub and the concrete surface is present, the deformation of the T-stub at the bolt position is given by the formula derived based on the equations (4) and (6).

$$\delta_T = \frac{F}{E}\left(\frac{4\ k_p(\lambda+1)^3 + k_b\ \lambda^2(4\ \lambda+3)}{16\ k_p\left(k_p + k_b\ \lambda^2\ (\lambda+3)\right)} \right) \tag{14}$$

The previous formula was written using parameters β and λ defined below

$$\beta = t / m, \tag{15}$$

$$\lambda = n / m. \tag{16}$$

Stiffness of the T-stub in case of the contact with the concrete surface is

$$k_T = \frac{F}{E\,\delta_T} = \left(\frac{16\,k_p\left(k_p + k_b\,\lambda^2\,(\lambda+3)\right)}{4\,k_p\,(\lambda+1)^3 + k_b\,\lambda^2\,(4\,\lambda+3)} \right) \tag{17}$$

Figure 3 The boundary of the prying action

The boundary between the cases with contact and exclusive of the contact, see Figure 2, can be evaluated for prying force $Q = 0$, which is

$$\lambda_{lim} = \frac{k_p}{3\,k_b}, \tag{18}$$

which may be written as

$$L_{b.lim} = \frac{7\,m^2\,n\,A_s}{\ell_{eff}\,t^3}. \tag{19}$$

If, as a further assumption, n is equal to $1{,}25\,m$, see [6], then

$$L_{b.lim} = \frac{8{,}82\,m^3\,A_s}{\ell_{eff}\,t^3}. \tag{20}$$

The above simplification of the boundary brings a qualitative error into the prediction. The accuracy of the simplification is shown on the following figures, see Figure 4a, 4b, and 4c

Three calculations with the T-stub were completed. The T-stub characteristics are $\ell_{eff} = 458{,}333\ mm$, $A_s = 480\ mm^2$, $m = 50\ mm$ and

- $L_b = 150\ mm$ (Figure 4a),
- $L_b = 300\ mm$ (Figure 4b),
- $L_b = 600\ mm$ (Figure 4c),

while the n / m ratio takes the following values: *0,5; 1,0; 1,5* and *2.0*.

The boundary between "prying" and "no prying" is computed by means of formulae (19) and (20) for the theoretical and simplified models respectively.

Figure 4a Comparison between the theoretical and simplified modelling of the boundary of prying, the stiffness prediction for variable thickness ratio t / m, $L_b = 150\ mm$

Figure 4b Comparison between the theoretical and simplified modelling of the boundary of prying, the stiffness prediction for variable thickness ratio t / m, $L_b = 300\ mm$

Figure 4c Comparison between the theoretical and simplified modelling of the boundary of prying, the stiffness prediction for variable thickness ratio t / m, L_b = 600 mm

3 Bending Stiffness

The prediction of the base plate stiffness may be based on the Annex J structure of formulae. It is assumed the components are independent in case of prying, see [6], Stiffness of the components is

if $$\frac{A_s}{L_b} \geq \frac{\ell_{eff.ini}\, t^3}{8{,}82\, m^3} \tag{21}$$

$$k_{p.EC3} = \frac{\ell_{eff.ini}\, t^3}{m^3} = \frac{0{,}85\, \ell_{eff}\, t^3}{m^3} \tag{22}$$

$$k_{b.EC3} = 1{,}6\, \frac{A_s}{L_b} \tag{23}$$

and in case of no prying

$$\frac{A}{L} \leq \frac{\ell_{C..Bsb}\, t^3}{8{,}82\, m^3} \tag{24}$$

$$k_{p.*} = \frac{F_p}{E\, \delta_p} = \frac{\ell_{eff.ini}\, t^3}{2\, m^3} = \frac{0{,}425\, \ell_{eff}\, t^3}{m^3} \tag{25}$$

$$k_{b.s} = \frac{F_b}{E\ \delta_b} = 2{,}0\ \frac{A_s}{L_b} \tag{26}$$

The stiffness of the components of the base plate in bending (22), (25) and the bolts in tension (23), (26) should be composed into stiffness of the T-stub

$$1 / k_T = 1 / k_{b.i} + 1 / k_{p.i}\ . \tag{27}$$

The influence of the washer plate is limited to 5% of the deformation [7] and could be neglected in the practical design.

3 Design Resistance

In the Eurocode 3 [4], three collapse mechanisms are derived. The design resistance of a T-stub corresponding to the collapse modes is the following:

Mode 3 - bolt fracture, see Figure 5a,

$$F_{3.Rd} = \Sigma\ B_{t.Rd} \tag{28}$$

Mode 1: plastic mechanism of the plate, see Figure 5b,

$$F_{1.Rd} = \frac{4\ \ell_{eff}\ m_{pl.Rd}}{m} \tag{29}$$

Mode 2 - mixed failure, see Figure 5c,

$$F_{2.Rd} = \frac{2\,\ell_{eff}\,m_{pl.Rd} + \Sigma\,B_{t.Rd}\,n}{m+n} \tag{30}$$

Figure 5 Failure modes of the T-stub

The design resistance F_{Rd} of the T-stub is derived as the smallest value obtained from the expressions (28) to (30)

$$F_{Rd} = min(F_{1.Rd}, F_{2.Rd}, F_{3.Rd}). \tag{31}$$

In particular case of base plates, it may happen that the elongation of the anchor bolts in tension in comparison to the flexural deformability of the base plate is such large, that no prying forces develop at the extremities of the T-stub flange. In this case, the failure results either from the anchor bolts in tension (Mode 3) or from yielding of the plate in bending, see Figure 5, where two hinges mechanism develops in the T-stub flange. This failure is not likely to appear in the beam-to-column joints and beam splices because of the limited elongation of the bolts in tension. This particular failure mode can be named Mode 1*, see Figure 6.

Figure 6 The mode 1 failure*

Figure 7 The T-stub design resistance

The corresponding resistance writes

$$F_{1^*.Rd} = \frac{2\,\ell_{eff}\,m_{pl.Rd}}{m} \tag{32}$$

If the Mode 1* mechanism forms large base plate deformations develop, which may result finally in the contact between the concrete block and the extremities of the T-stub flange, i.e. in the prying forces. Further loads may therefore be applied to the T-stub until failure is obtained through Mode 1 or Mode 2. However, to reach this level of the resistance, it is necessary to develop very large deformations of the T-stub, which are not acceptable for design conditions. The additional strength which separates Mode 1* from Mode 1 or Mode 2 is therefore disregarded and Formula (32) is applied despite the discrepancy which could result from the comparisons with some experimental results [16].

As a result, in cases where no prying forces develop, the design resistance of the T-stub is taken as equal to

$$F_{Rd} = min\left(F_{1^*.Rd}, F_{3.Rd}\right), \tag{33}$$

when $F_{3.Rd}$ is given by formula (28).

The influence of cover plate on the failure Mode 1 based on study [6], aimed at strengthening of the base plate, is also considered [4]. The collapse mode 1 is applicable with the approved bending resistance [8]

$$F_{1.Rd} = \frac{\ell_{eff.1}\,(4\,m_{ef.Rd} + 2\,m_{le.Rd})}{m}, \tag{34}$$

for

$$m_{bp.Rd} = 0{,}25\,t_{bp}^2\,f_{y.bp} / \gamma_{M0}, \tag{35}$$

where

$f_{y.bp}$ is the yield stress of the cover plate,

t_{bp} is the thickness of the cover plate.

4 T-stub Effective Length

Eurocode 3 [4] distinguishes between so-called circular and non-circular yield line mechanisms in T-stub flanges (see Figure 8a). These differ by their shape and lead to specific values of the T-stub effective lengths noted respectively $\ell_{eff.cp}$ and $\ell_{eff.np}$. The major difference between the circular and non-circular patterns is linked to development of the prying forces between the T-stub flange and rigid foundation The circular patterns form without any development of prying forces Q and the reverse happens for the non-circular ones. The direct impact on the different possible failure modes is as follows:

Mode 1

The presence or not of the prying forces do not alter the failure mode which is linked in both cases to development of a complete yield mechanism of the plate. Formula (26) applies therefore to the circular and non-circular yield line patterns.

Mode 2

The bolt fracture clearly results from over-loading of the bolts in tension because of the prying effects; therefore Mode 2 occurs only in the case of non-circular yield line patterns.

Mode 3

This mode does not involve any yielding of the flange and applies therefore to any T-stub.

As a conclusion, the calculation procedure differs according to the yield line mechanisms developing in the T-stub flange (7):

$$F_{Rd} = min(F_{1.Rd}; F_{1.Rd}) \qquad \text{for the circular patterns} \tag{36}$$

$$F_{Rd} = min(F_{1.Rd}; F_{2.Rd}; F_{3.Rd}) \quad \text{for the non-circular patterns} \tag{37}$$

Figure 8 The patterns of the failure, a) circular pattern, b) non-circular pattern

All the possible yield line patterns are considered through the recommended values of the effective lengths of the T stub. They are grouped into two categories: circular and non-circular patterns. The minimum values of the effective lengths - respectively termed $\ell_{eff.cp}$ and $\ell_{eff.np}$ - are therefore selected for category. The failure load is then derived, by means of Formula (31), by considering successively all three possible failure modes, but with the specific values of the effective length:

Mode 1: $\ell_{eff,1} = min(\ell_{eff,cp}; \ell_{eff,np})$ (38)

Mode 2: $\ell_{eff,2} = \ell_{eff,np}$ (39)

Mode 3: $\ell_{eff,3} = \ell_{eff,2} = \ell_{eff,np}$ (40)

Concerning Mode 1* failure, only circular patterns have therefore to be taken into consideration and the non-circular patterns have to be disregarded. Mode 1* identifies then exactly to Mode 1 and, in order to ensure that the design resistances provided by formulae (29) and (32) are equal, the effective lengths for the circular patterns defined in revised Annex J have to be multiplied by a factor 2 before being implemented in the Formula (29).

Besides that, the non-circular patterns not involving prying forces in the bolts may occur. These ones may be considered through Formula (29), but the appropriate effective length characteristics should be introduced. The lowest of the effective lengths between those derived for the circular and non-circular patterns respectively is that which will determines the design resistance of the T-stub. Table 1 indicates how to select the values of ℓ_{eff} for two classical base plate configurations, in the cases where the prying forces develop and do not develop.

Figure 9 The effective length ℓ_{eff} of a T stub for the base plate with two bolts inside the flanges

Table 1 The effective length ℓ_{eff} of a T stub for the base plate with two bolts inside the flanges

Figure 10 The effective length ℓ_{eff} of a T stub for the base plate with four bolts outside the flanges

Table 2 Effective length ℓ_{eff} of a T stub for base plate with four bolts

Figure 10 Basic types of anchoring; cast-in-place (a), undercut (b), adhesive (c), grouted (d), expansion (e), anchoring to grillage beams (f)

5 Anchor Bolts

The typical fixing of the anchor bolts into the concrete block are for instance: hooked bars for light anchoring, cast-in-place headed anchors and anchors bounded to drilled holes, see Figure 11. The more expensive anchoring systems such as "grillage beams embedded in concrete" are designed for large frames. The models of the anchoring design resistance compatible with the Eurocode safety have been prepared [12] for the short anchoring used in concrete structures and are applicable to the long anchors used in the structural steel.

The anchoring resistance is based on the ultimate limit state concept. The resistance of the structural steel anchors has to be such that the anchor bolts fail in tension before the anchorage (pullout of the anchor, failure of the concrete, ...) reach its own resistance. It assures ductile behaviour of the anchor bolt. The recommendations and good practice of base plates designed for seismic areas require failure of the base plate to prevent failure of the anchor bolt [13].

For a single anchor, the following failure modes have to be considered:

- The pull-out failure $N_{p.Rd}$,
- The concrete cone failure $N_{c.Rd}$,
- The splitting failure of the concrete $N_{sp.Rd}$.

Similar verifications are required for anchor bolt groups.

The detailed complex description of the evaluation formulae for the design resistance of various types of fastenings in the tension is included in the CEB Guide [12]. When calculating the anchoring resistance, the tolerances for the position of the bolts should be taken into account according to Eurocode 3, Clause 7.7.5 [4]. This recommendation should complicate the prediction of the resistance and the stiffness. It may result in developments of different models of prediction for different load cases, which is not acceptable in the practical design. The studies [8] shows small differences for the stiffness as well as resistance prediction. The tolerances higher than recommended in standards [14] should be introduced into the prediction only.

In case of embedded anchor bolts, the effective free length L_b consist of the physical free length L_{bf} and the embedded free length $L_b = L_{bf} + L_{be}$, see Figure 11.

Figure 12 The anchor bolt effective free length

The headed anchor bolt can be use as a reference for the modelling of the typical long embedded anchor bolts that are preferably used in steel structures. The deformation of the anchor bolt includes the steel bolt elongation δ_b, the concrete cone deformation δ_c, and the elongation due to the bolt head deformation δ_h.

$$\delta = \delta_b + \delta_c + \delta_h. \tag{41}$$

The calculation can be simplified taking into account only the steel bolt elongation for long anchor bolts used in structural steel. The prediction of embedded free length of typical structural bolts can be based on assumption of the distribution of the bound stresses [15]. The relative displacement δ between the surface of the concrete foundation and the embedded bar subjected to tensile force has been observed experimentally by [11]. Based on these experimental observations, the length L_t, at which the tensile stress in the bar decreases to zero value is seen to be approximately equal to *24 d*. This length may vary during the loading because of the local looses of the bound resistance between the steel bar and the concrete block. In the calculations of the stiffness properties of the anchor bolts in tension, a constant stress in the bar σ is assumed to act on a equivalent free length L_{be}, see Figure 13b. The deformation of the bolt δ is expressed as

$$\delta = \frac{B\, L_{be}}{E\, A_s}. \tag{42}$$

If σ_{bx} designates the bond stress between the concrete and the embedded bar, the axial stress σ along the bar writes:

$$\sigma_x = \sigma - \int_0^x \frac{4\, \sigma_{bx}}{d}\, dx\,, \tag{43}$$

Figure 13 Bond stress distribution for the long embedded bar

The stress on the bar of length L_{em} is

$$\sigma = \int_0^{L_t} \frac{4\,\sigma_{bx}}{d}\,dx. \tag{44}$$

Substituting the strain $\varepsilon_x = \sigma_x / E$, the following can be obtained

$$E\varepsilon_x = \int_x^{L_t} \frac{4\sigma_{bx}}{d}dx. \tag{45}$$

and

$$\delta = \int_0^{L_t} \varepsilon_x\,dx = \frac{4}{dE}\int_0^{L_t}\int_x^{L_t} \sigma_{bx}\,dx^2. \tag{46}$$

If σ_{bx} is constant and independent of x, see Figure 13b, the elongation of the bolt is

$$\delta = \frac{2\,\sigma_b\,L_{em}^2}{d\,E}. \tag{47}$$

Assume the length L_{em} is proportional to bolt diameter d and the length $L_t \cong 24\,d$, then

$$\sigma_b = \frac{\sigma\,d}{4\,L_t}, \tag{48}$$

and the elongation of the bolt at the concrete surface is

$$\delta = \frac{2\,\sigma_b\,L_{em}^2}{d\,E} = \frac{2\,\sigma\,d\,L_{em}}{4\,d\,L_t\,E} = \frac{\sigma\,L_{em}}{2\,E}, \tag{49}$$

$$\delta = \frac{F_b\,L_t}{E\,A}, \tag{50}$$

finally

$$L_{be} = \frac{L_{em}}{2} = 12\,d\,. \tag{51}$$

Figure 14 The linear, triangular model of bond stress for the long embedded bar

If the bond stress varies linearly, as shown in the Figure 14,

$$\delta = \frac{2\,\sigma_{b0}\,L_{em}^2}{3\,d\,E}. \tag{52}$$

In case of the elongation δ proportional to the bolt diameter d

$$\sigma_{b0} = \frac{\sigma\,d}{2\,L_{em}}, \tag{53}$$

it is possible to express the equivalent length

$$L_{be} = \frac{L_{em}}{3} = \frac{24\,d}{3} = 8\,d\,. \tag{54}$$

Figure 15 The non-linear distribution of the bond stress

If the bond stress varies non-linearly, as shown in Figure 15, the shape can be estimated by the cubic parabola

$$\delta \cong \frac{2\,\sigma_{b0}\,L_t^2}{5\,d\,E} \tag{55}$$

In case of δ proportional to d the equation can be rewritten for the conservative value of the equivalent length

$$L_{be} = \frac{L_t}{5} = \frac{24\,d}{5} = 4{,}8\,d\,. \tag{56}$$

The analytical prediction of the embedded anchor bolt elongation is sensitive to prediction of the distribution of the stress along the anchor bolt. The FE sensitivity study, was streamed to show the influence of the anchor bolt length and the headed plate during elastic deformations at the concrete surface, see Figure 16. The sensitivity study was based on experiments [16] and [17]. The contact elements (point to surface) are used to simulate the development of the contact stresses.

Based on this study, the embedded free length of the bolts with regular surface can be predicted as $L_{be} \cong 8\,d$ for the long typical structural embedded. The stress is developed at the length of $24\,d$, which may be expected as a boundary length of the anchoring by a long bolt.

This length is reduced by the haunch or by the headed plate. The anchor bolt area can be taken as net area A_s to simplify the design.

Figure 16 A quarter of FE mesh for simulation of the anchor bolt, see test [16], bolt is connected by point to surface contact elements, development of contact stress

6 Validation

Special set of the component experiments was carried out at Czech Technical University in Prague to evaluate a component prediction [16] and [17]. The main parameters of the tests are the bolt M 24 with the cut thread and base plate of thickness 12 or 20 mm and size 150, 190, and 210 × 100 mm resulting in dimension of the T-stub m = 32 , 52 and 67 mm, n = 40 mm. The size of the concrete block was 550 × 550 × 550 mm.

Figure 17 Comparison of the proposed model to experiments with the anchor bolts [17], f_{ck} = 40,1 MPa

Figure 18 Comparison of the proposed model to experiments with the anchor bolts [16], f_{ck} = 33,3 MPa

The anchor bolts tests, see Figure 17 and 18, show a good agreement with the proposed model for the anchor bolt stiffness.

The experimental programme consists of twelve tests with T-stub in tension [16]. The experimental programme was streamed to evaluation of prying effect, strength and stiffness of the T-stub. For this purpose, the base plate thickness and the bolt pitch were the only variable parameters, the other characteristics of the specimens were kept constant. Six specimens were designed with the thick base plate ($t = 20\ mm$), the others with thin base plate ($t = 12\ mm$). The bolt pitch was 110 mm, 140 mm and 170 mm, see Figure 19.

In addition, two pullout tests of single anchor bolt were carried out to obtain tension stiffness and resistance of the anchor bolts, see Figure 18.

Figure 19 The test specimen for the experiments with the T-stub

The pictures show the test results of the T-stub with the bolt pitch 110 mm and the different base plate thickness. The comparison of the complex and simplified calculations to the experimental results is included. The calculated resistance of specimens with the thin base plate is the same for both models and is in good agreement with the experiments see Figure 21. The combination of the plate mechanism and breaking of the anchor bolts reached the collapse of both specimens, which corresponds to Mode 2 of the design model.

The resistance of the specimens W97-01 and W97-02 with the thicker base plate differs for complex and simplified models see Figure 20. According to the simplified model there is prying of anchor bolts, which results in the higher resistance. The complex model predicts no prying of the anchor bolts, which corresponds to the experimental observations. There were no plastic hinges in the base plate during the experiment and the tension resistance of anchor bolts limits the resistance. However, the collapse was not reached because of the limitation of the loading cell. The predicted stiffness is in a good agreement for all tests.

Figure 20 The load deflection diagram of experiments W97-01 and W97-02, plate thickness 20 mm

Figure 21 The load deflection diagram of experiments W97-05 and W97-06, plate thickness 12 mm

Another four tests were performed with increased bolt pitch, see Figure 22 and Figure 23. The prying of the anchor bolts occurred in both cases, for experiments with thin and thicker base plates and it corresponds to simplified and complex models. There is a good agreement between the experimental and calculated resistances.

The creation of two plastic hinges in the base plate of the specimens W97-03 and W97-04, see Figure 22, with thick base plate was clearly observed during the experiment, but the anchor bolts of the specimens finally collapsed. The other specimens with thin base plate collapsed when four plastic hinges created in the base plate After that the testing was stopped due to achieving the very large uplift, about 8 mm. The experiment W97-07, see Figure 23, was interrupted by the splitting failure of the concrete block without reinforced.

Figure 22 The load deflection diagram of experiments W97-03 and W97-04, plate thickness 20 mm

Fig 23 The load deflection diagram of experiments W97-07 and W97-08, plate thickness 12 mm

The last four specimens with the largest bolt pitch 170 mm showed the similar behaviour during the test. The high influence of the prying of the anchor bolts was observed, which guided the combined collapse of the anchor bolts and the yielding of the base plate with the creation of four plastic hinges, i.e. collapse mode 2. There was only difference on ductility of the T-stub. The specimens W97-11 and W97-12, see Figure 24, with thick base plate allowed uplift of about 9 mm followed by collapse of anchor bolts. The specimen W97-09 collapsed by splitting failure of the concrete block, collapse of W97-10 was not reached, , see Figure 25,. However, the uplift of both specimens was about 20 mm. The bending and the bearing of the anchor bolts ware also observed under the extremely high deformations but it did not influence the collapse.

Figure 24 The load deflection diagram of experiments W97-11 and W97-12, plate thickness 20 mm

Figure 25 The load deflection diagram of experiments W97-09 and W97-10, plate thickness 12 mm

7 Conclusions

- The base plate in bending and anchor bolt in tension is the component guiding the behaviour of column bases.
- The boundaries of two types of behaviour, with contact of base plate to the concrete surface and without this contact, can be predicted by simple analytical way with a good

accuracy. The resistance and the stiffness of the component can be calculated for both types of behaviour.

- The embedded free length of the anchor bolt is the most important parameter for stiffness prediction, which may be seen at the presented study. The embedded free length can be predicted as $L_{be} \cong 8\,d$ for typical structural embedded bolts with regular bolt surface.

Acknowledgement

Within the framework of the activities of the COST C1 European Project (Semi-rigid behaviour of civil engineering structural connections) and the Technical Committee 10 of ECCS (European Steel Fabricator Association), an ad-hoc working group was established to prepare a background document for European standardisation and a European design manual for column bases. Members of this group are: D. Brown, SCI London; A. M. Gresnigt, TU Delft; J. P. Jaspart, University of Liège; Z. Sokol, CTU in Prague; J. W. B. Stark, TU Delft; C. M. Steenhuis, TU Eindhoven; J. C. Taylor, SCI London; F. Wald, CTU in Prague (Convenor of the group), K. Weynand, RTWH Aachen. The work at this contribution has been supported by the grant No. MŠMT 21 000 000 1.

References

[1] Treiberg, T.: in Swedish. Base plates. Staalbyggnadsinstitutet, Pub. 101, Stockholm 1987. p. 99.

[2] Akiyama H.: *Seismic Design of Steel Column for Architecture.* in Japanese, Gibodoskupan, Tokyo 1985.

[3] Melchers R. E.: *Modelling of Column-Base Behaviour.* In Connections in Steel Structures, behaviour, strength and design, Proceedings, ed. Bjorhovde R., Brozzetti J., Colson A., Elsevier Applied Science, London 1987, pp. 150-157.

[4] Eurocode 3, ENV - 1993-1-1, *Design of Steel Structures - General rules and roles for buildings.* CEN, Brussels 1992; including Part 1.1, A2: *Design of Steel Structures - General rules and roles for buildings, Annex J,* European Prenorm, CEN, Brussels 1998.

[5] Zoetemeijer, P.: Summary of the researches on bolted beam-to-column connections. Report 6-85-7, University of Technology, Delft, The Netherlands 1985.

[6] Jaspart, J. P. : Etude de la semi-rigidité des noeuds poutre-colonne et son influence sur la résistance et la stabilité des ossatures en acier. Ph.D. Thesis, Department MSM, University of Liège 1991.

[7] *Column Bases in Steel Building Frames,* COST C1, ed. K. Weynand, Brussels 1999.

[8] Wald F.: *Patky Sloupů - Column Bases*, ČVUT, Prague 1995, p. 137, ISBN 80-01-01337-5.

[9] Yee, Y. L., Melchers, R. E.: Moment rotation curves for bolted connections. *Journal of the Structural Division*, ASCE, Vol. 112, ST3, pp. 615-635, March 1986.

[10] Owens G. W., Cheal B. D.: *Structural Steelwork Connections.* Butterworths, London 1988.

[11] Wald F., Obata M., Matsuura S., Goto Y.: *Prying of Anchor Bolts.* Nagoya University Report, Nagoya 1993, pp. 241 - 249.

[12] *Fastenings to Concrete and Masonry Structures.* State of the Art Report, CEB, Thomas Telford Services Ltd, London 1994, p. 248, ISBN 0 7277 1937 8.

[13] Astaneh a., Bergsma g., Shen j.h.: *Behavior and Design of Base Plates for Gravity, Wind and Seismic Loads.* in Proceedings AISC, National Steel Construction Conference, June, Las Vegas 1992.

[14] ENV 1090-1, *Execution of steel structures, Part 1 - General rules and rules for buildings.* CEN, Brussels 1997.

[15] Salmon C. G., Schenker L., Johnston G. J.: *Moment - Rotation Characteristics of Column Anchorages.* Transaction ASCE, 1957, Vol. 122, No. 5, pp. 132 - 154.

[16] Sokol Z., Wald F.: *Experiments with T-stubs in Tension and Compression.* Research Report, ČVUT, Prague 1997.

[17] Wald F., Šimek I., Sokol Z., Seifert J.: *The Column-Base Stiffness Tests.* in Proceedings of the Second State of the Art Workshop COST C1, ed. Wald F., Brussels 1994, pp. 281 - 292.

[18] Sokol Z., Ádány S., Dunai L., Wald F.: *Column Base Finite Element Modelling.* Acta Polytechnica, Vol. 39, No:5, Praha 1999, ISBN 1210-2709.

Mr. D. Brown
The Steel Construction Institute
Silwood Park
Ascot-Berkshire SL5 7QN
United Kingdom
tel: 44 1344 623 2233
fax: 44 1344 622 944
d.brown@steel-sci.com

Ing. Z. Sokol
Czech Technical University
Faculty of Civil Engineering
Department of Steel Structures
Thákurova 7
16629 Praha 6
Czech Republic
tel: 420 2 2435 4767
fax: 420 2 3117 466
sokol@fsv.cvut.cz

Dr. J. P. Jaspart
Université de Liège
Département MSM Institut du Génie Civil
Chemin des Chevreuils 1 (B52/3)
B-4000 Liège 1
Belgium

Doc. Ing. F. Wald, CSc.
Czech Technical University
Faculty of Civil Engineering
Department of Steel Structures
Thákurova 7
16629 Praha 6

tel: 32 4 366 9247
fax: 32 4 366 9192
jean-pierre.jaspart@ulg.ac.be

Czech Republic
tel: 420 2 2435 4757
fax: 420 2 3117 466
wald@fsv.cvut.cz

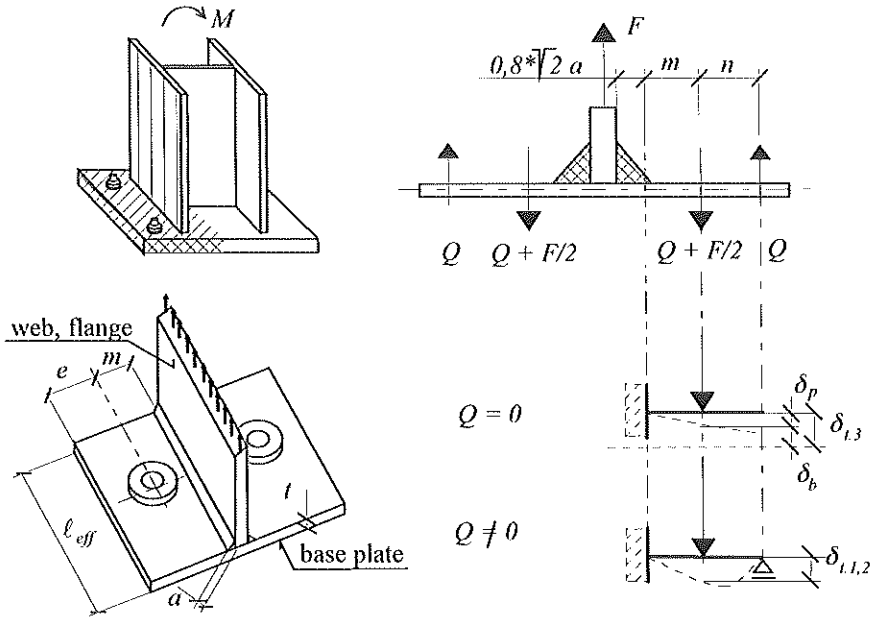

Figure 1 The T stub - anchor bolts in tension and base plate in bending, assumption of the acting forces and deformations

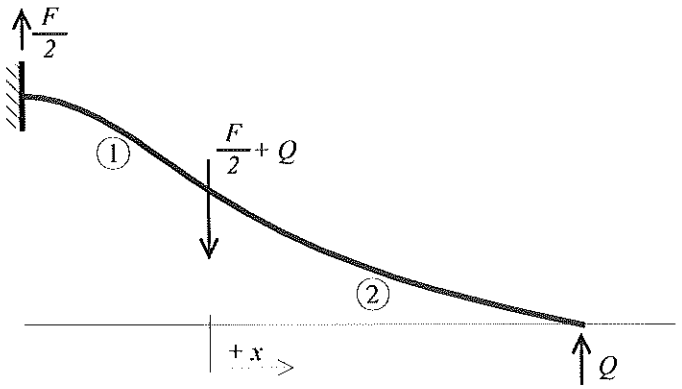

Figure 2 The beam model of the T-stub

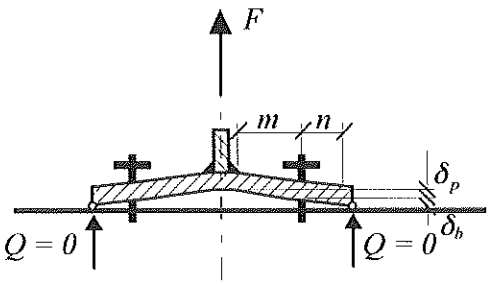

Figure 3 The boundary of the prying action

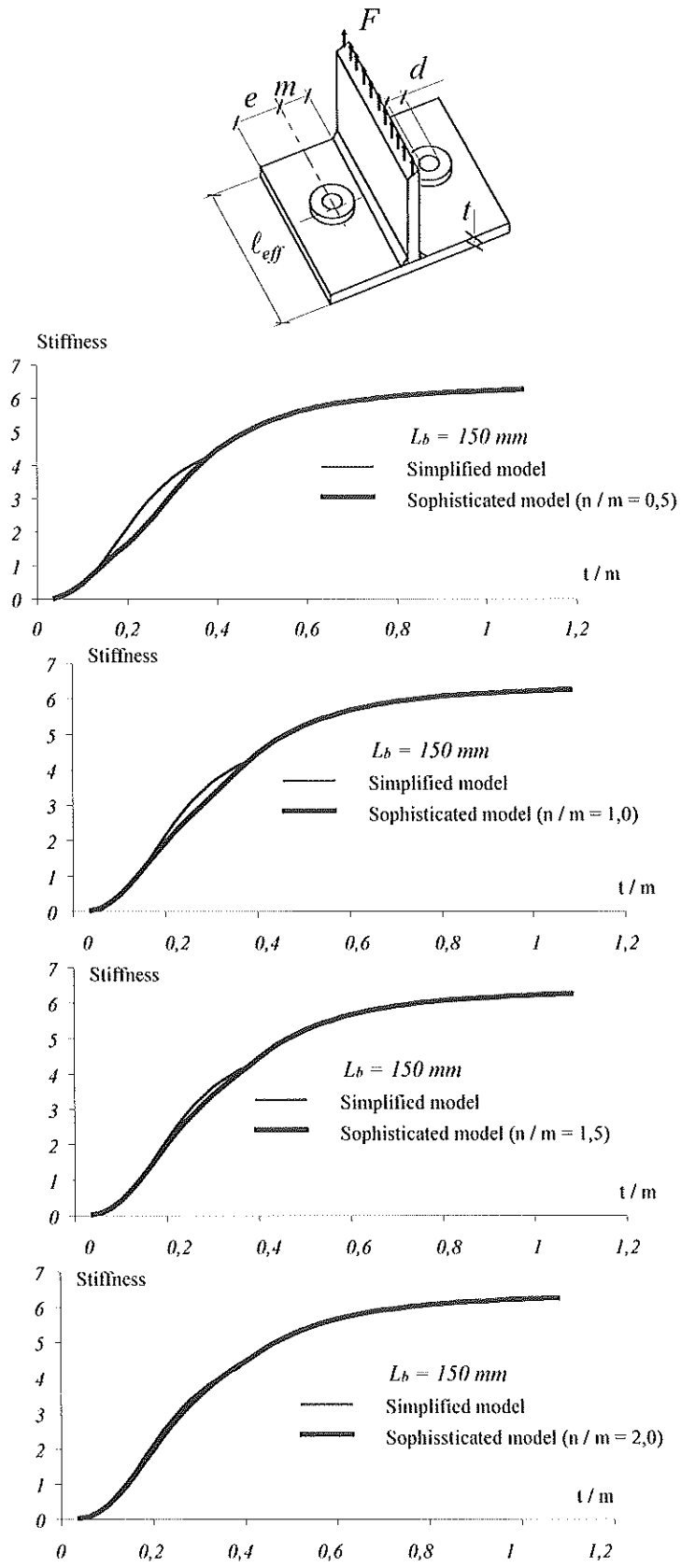

Figure 4a Comparison between the theoretical and simplified modelling of the boundary of prying, the stiffness prediction for variable thickness ratio t / m, L_b =150 mm

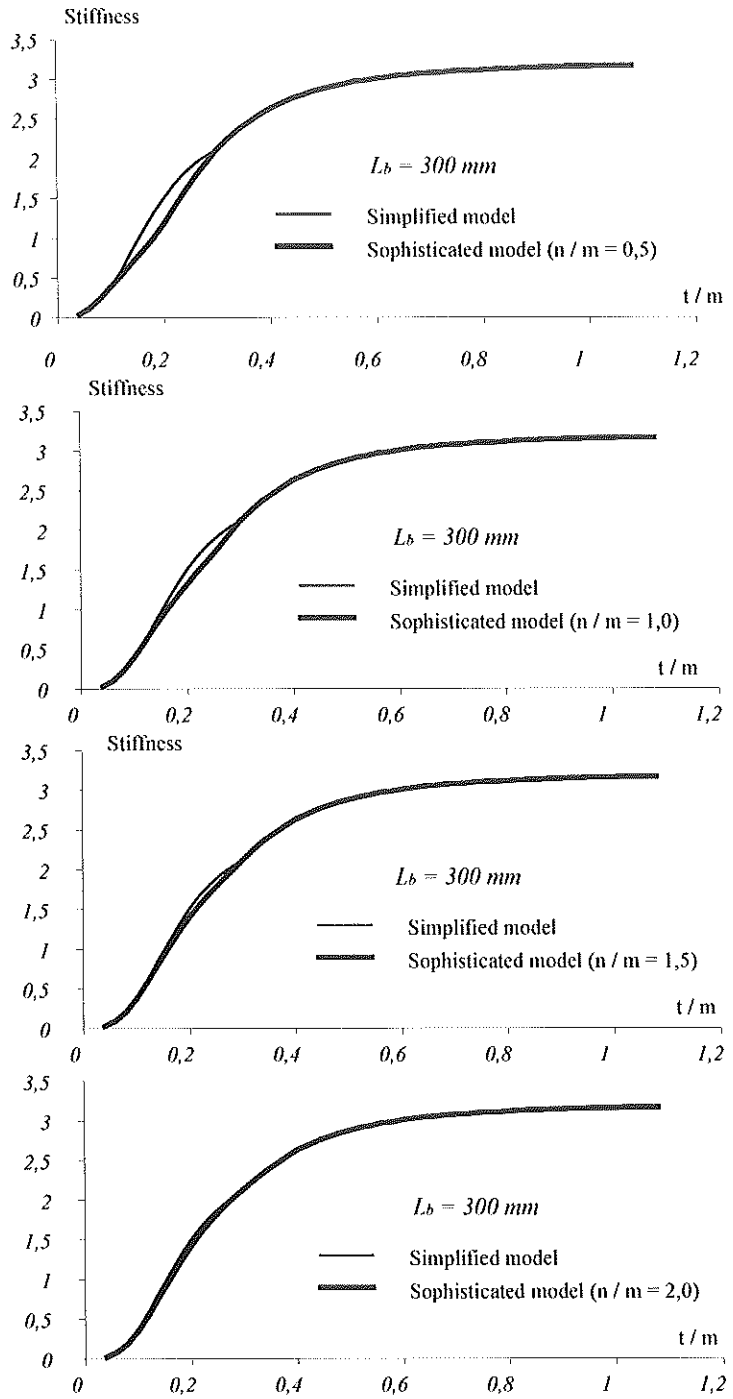

Figure 4b Comparison between the theoretical and simplified modelling of the boundary of prying, the stiffness prediction for variable thickness ratio t / m, L_b = 300 mm

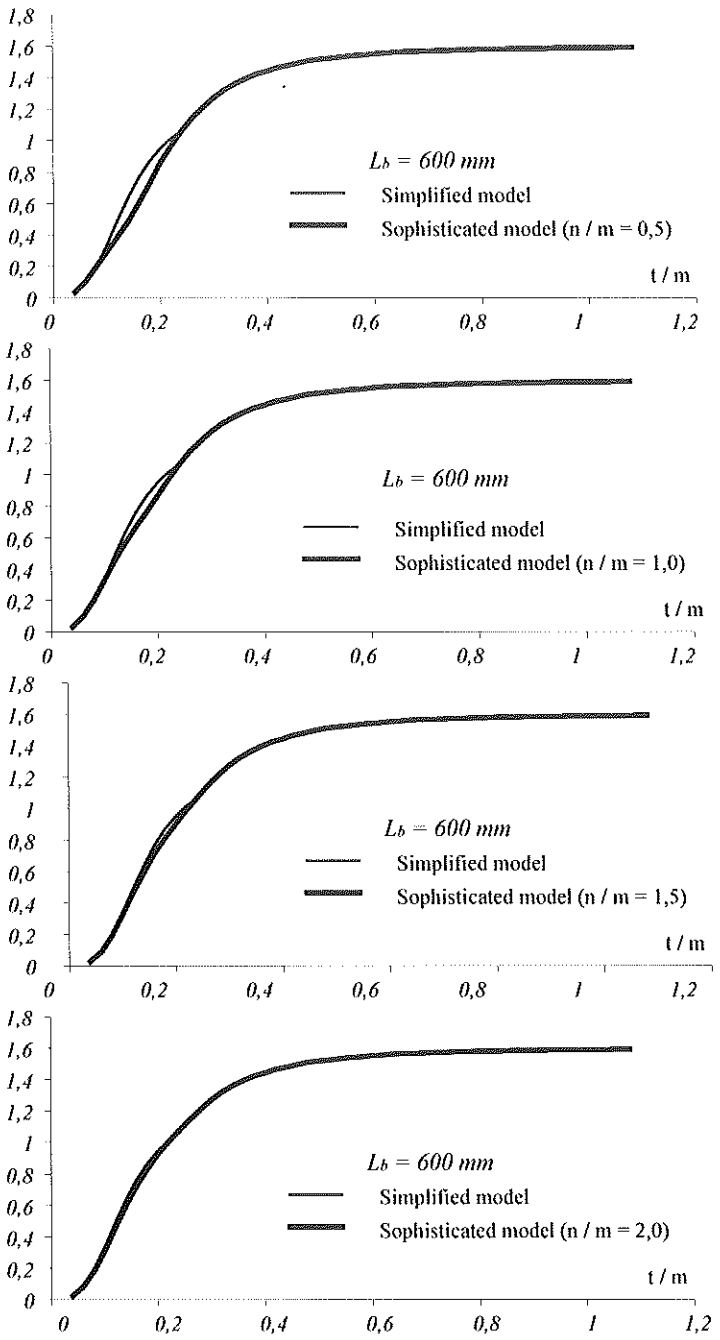

Figure 4c Comparison between the theoretical and simplified modelling of the boundary of prying, the stiffness prediction for variable thickness ratio t / m, L_b =600 mm

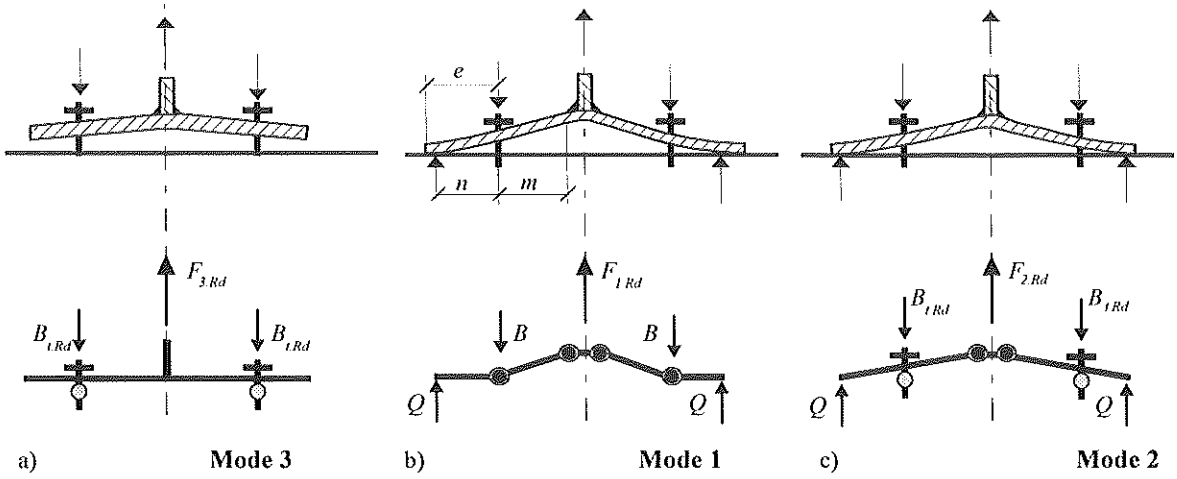

Figure 5 Failure modes of the T-stub

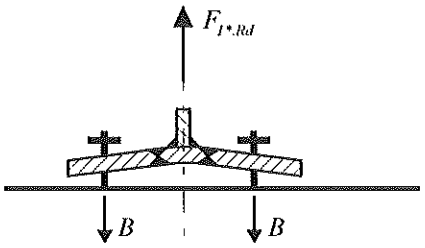

Figure 6 The mode 1 failure*

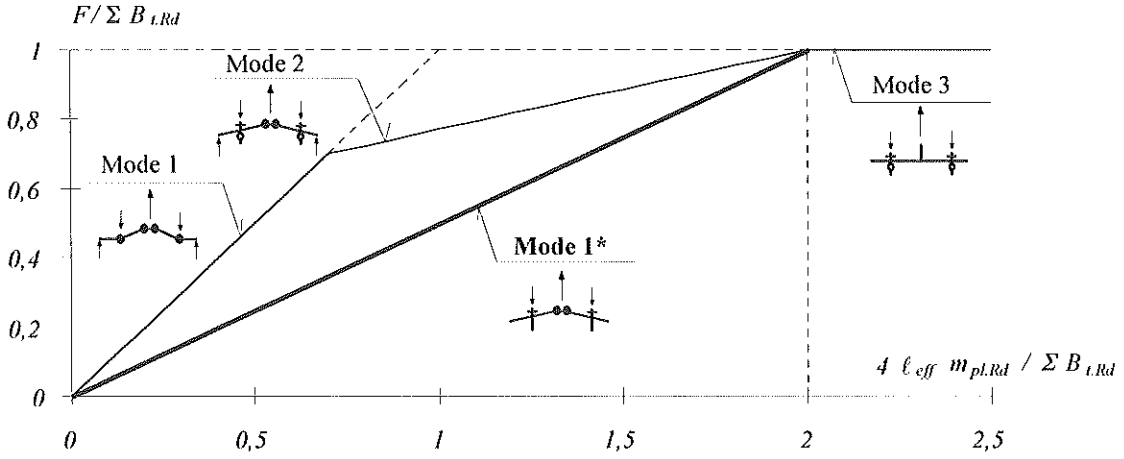

Figure 7 T-stub design resistance

a) Circular pattern, $\ell_{eff,cp}$ 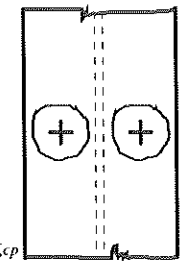 b) Non-circular pattern, $\ell_{eff,np}$ 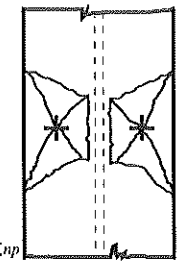

Figure 8 The patterns of the failure, a) the circular pattern, b) the non-circular pattern

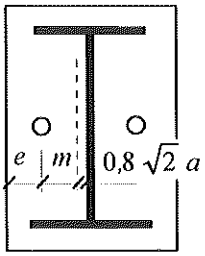

Figure 9 The effective length ℓ_{eff} of a T stub for the base plate with two bolts inside the flanges

Table 1 The effective length ℓ_{eff} of a T stub for the base plate with two bolts inside the flanges

Prying case	No prying case
$\ell_1 = 2\,\alpha\, m - (4\, m + 1{,}25\, e)$	$\ell_1 = 2\,\alpha\, m - (4\, m + 1{,}25\, e)$
$\ell_2 = 2\,\pi\, m$	$\ell_1 = 4\,\pi\, m$
$\ell_{eff.1} = \min(\ell_1; \ell_2)$	$\ell_{.ee\,2} = \min(\ell_2; \ell_1)$
$\ell_{eff.2} = \ell_1$	$\ell_{eff.2} = \ell_1$

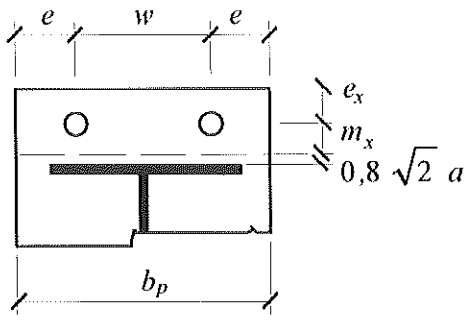

Figure 10 The effective length ℓ_{eff} of a T stub for the base plate with four bolts outside the flanges

Table 2 The effective length ℓ_{eff} of a T stub for the base plate with four outside the flanges

Prying case	No prying case
$\ell_1 = 4\ m_x + 1{,}25\ e_x$	$\ell_7 = 4\ m_x + 1{,}25\ e_x$
$\ell_2 = 2\ \pi\ m_x$	$\ell_7 = 4\pi m_x$
$\ell_3 = 0{,}5\ b_p$	$\ell_7 = 0{,}5\ b_p$
$\ell_4 = 0{,}5\ w + 2\ m_x + 0{,}625\ e_x$	$\ell_6 = 0{,}5\ w + 2\ m_x + 0{,}625\ e_x$
$\ell_5 = e + 2\ m_x + 0{,}625\ e_x$	$\ell_5 = e + 2\ m_x + 0{,}625\ e_x$
$\ell_6 = \pi\ m_x + 2\ e$	$\ell_4 = 2\ \pi\ m_x + 4\ e$
$\ell_7 = \pi\ m_x + p$	$\ell_7 = 2\ (\pi\ m_x + p)$
$\ell_{eff.1} = min\ (\ell_1;\ell_2;\ell_3;\ell_4;\ell_5;\ell_6;\ell_7)$	$\ell_{eff.1} = min\ (\ell_1;\ell_2;\ell_3;\ell_4;\ell_5;\ell_6;\ell_7)$
$\ell_{eff.2} = \min\ (\ell_7;\ell_2;\ell_3;\ell_4)$	$\ell_{eff.2} = \min\ (\ell_7;\ell_2;\ell_3;\ell_4)$

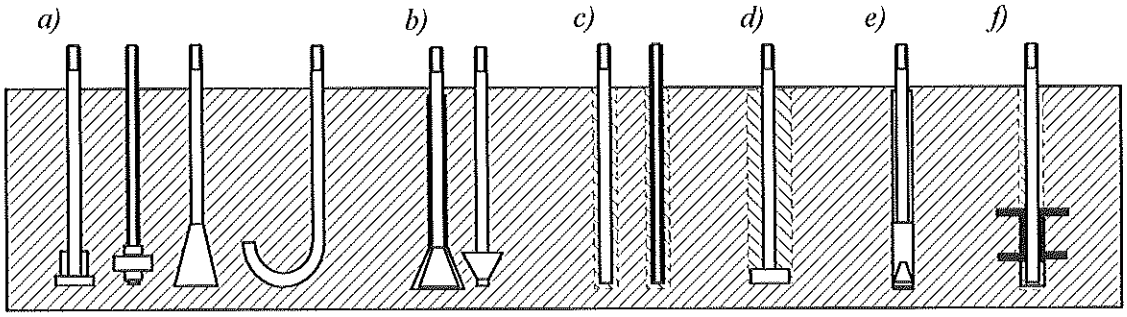

Figure 11 Basic types of anchoring; cast-in-place (a), undercut (b), adhesive (c), grouted (d), expansion (e), anchoring to grillage beams (f)

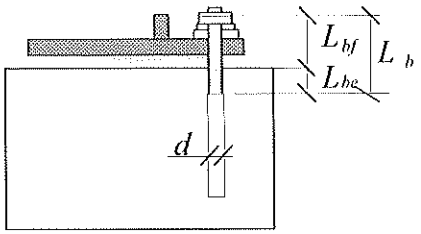

Figure 12 The anchor bolt effective free length

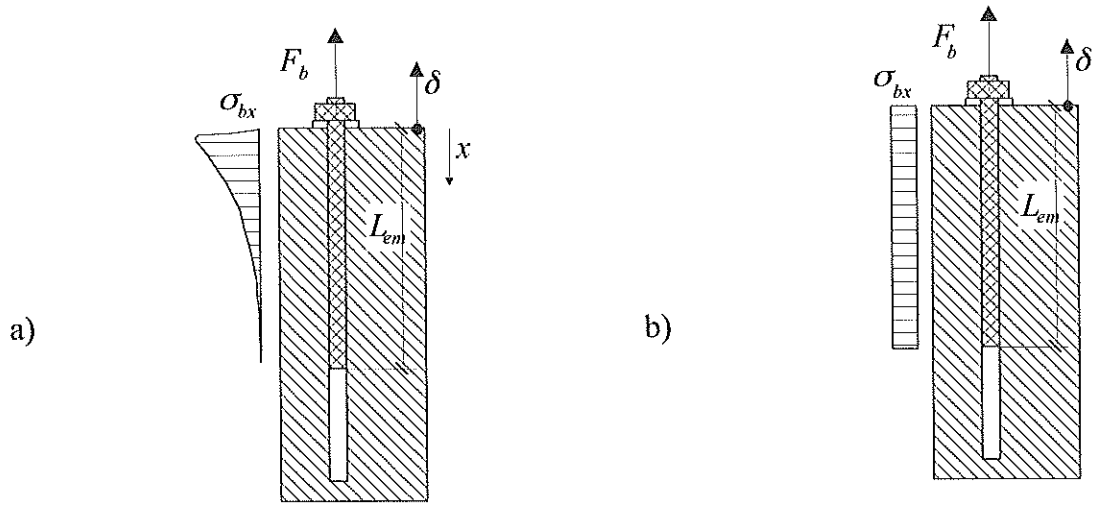

Figure 13 Bond stress distribution for the long embedded bar

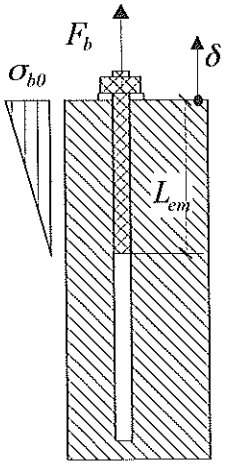

Figure 14 The linear, triangular model of bond stress for the long embedded bar

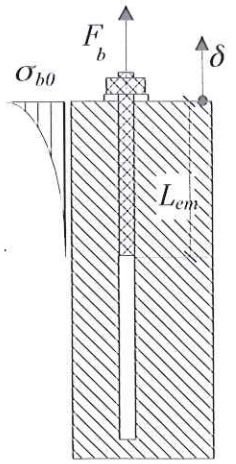

Figure 15 The non-linear distribution of bond stress

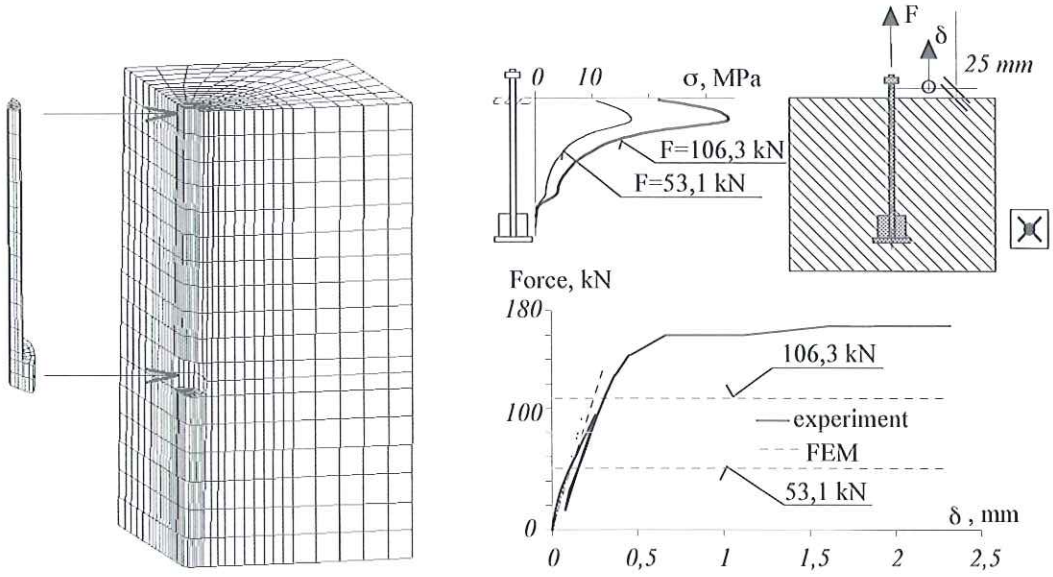

Figure 16 A quarter of FE mesh for simulation of the anchor bolt, see test [16], bolt is connected by point to surface contact elements, development of contact stress

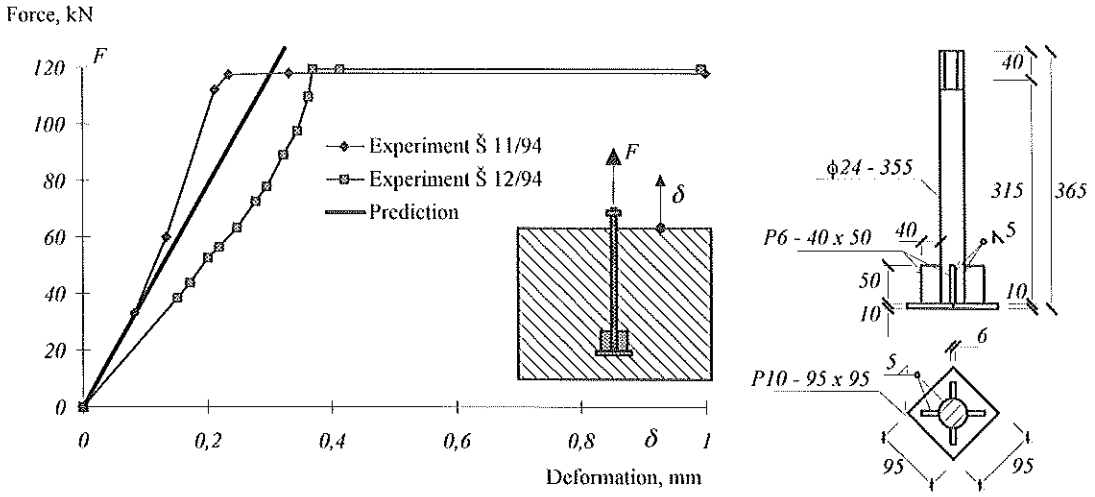

Figure 17 Comparison of the proposed model to experiments with the anchor bolts [17], f_{ck} = 40,1 MPa

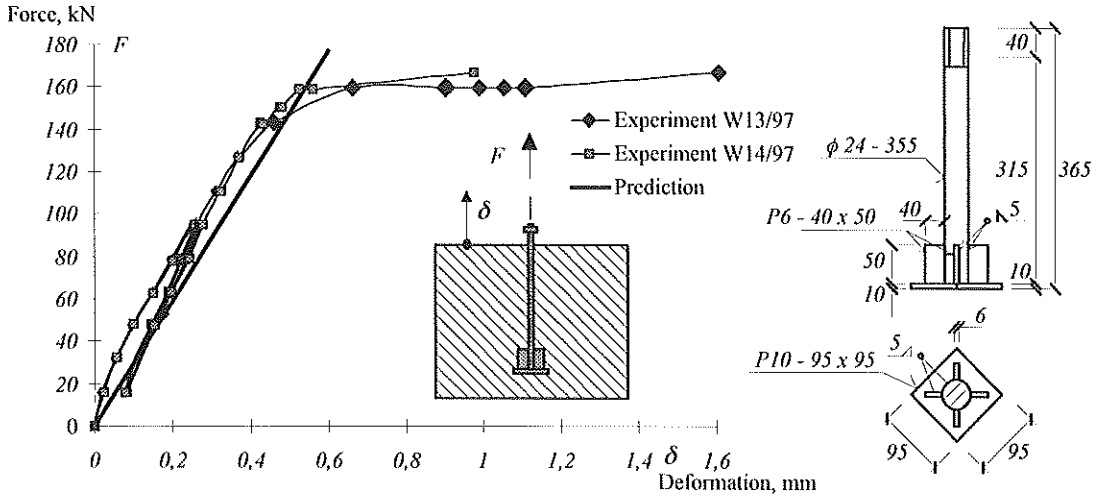

Figure 18 Comparison of the proposed model to experiments with the anchor bolts [16], f_{ck} = 33,3 MPa

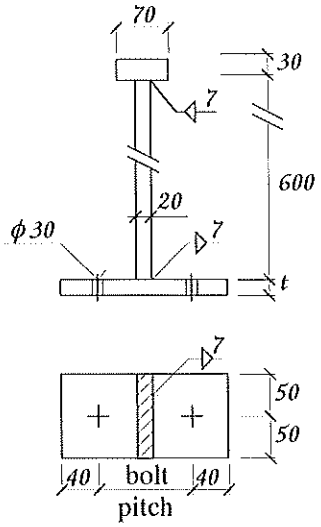

Figure 19 The test specimen for the experiments with the T-stub

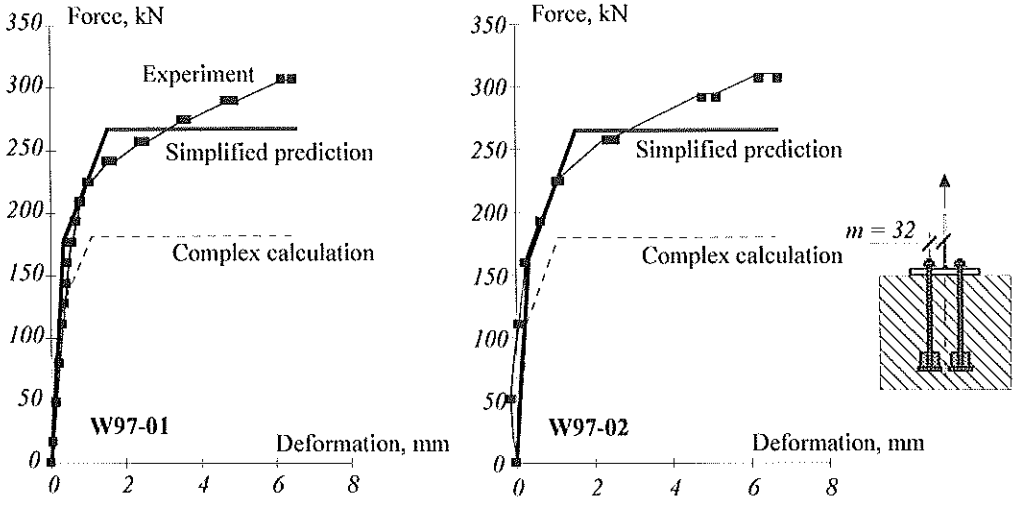

Figure 20 The load deflection diagram of experiments W97-01 and W97-02, plate thickness 20 mm

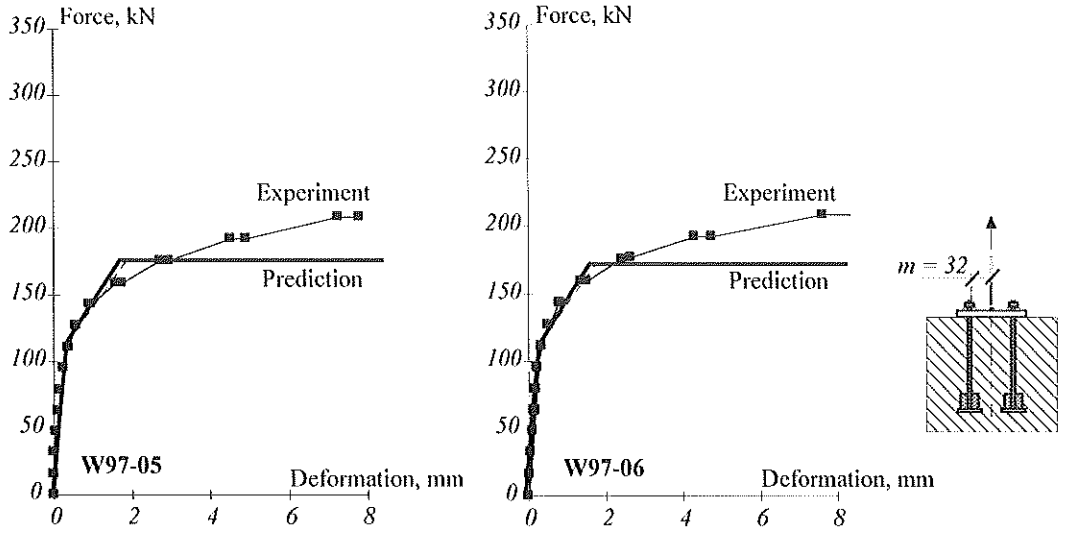

Figure 21 The load deflection diagram of experiments W97-05 and W97-06, plate thickness 12 mm

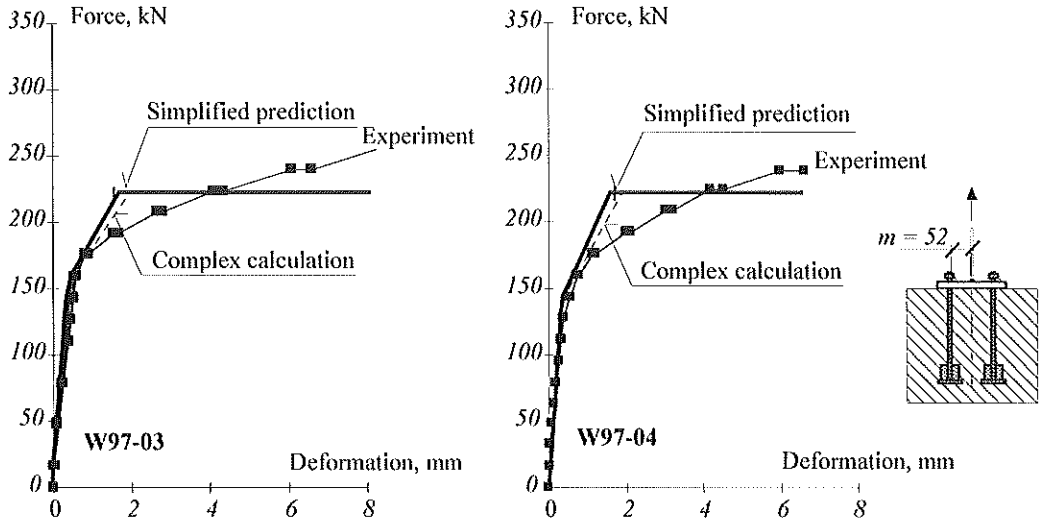

Figure 22 The load deflection diagram of experiments W97-03 and W97-04, plate thickness 20 mm

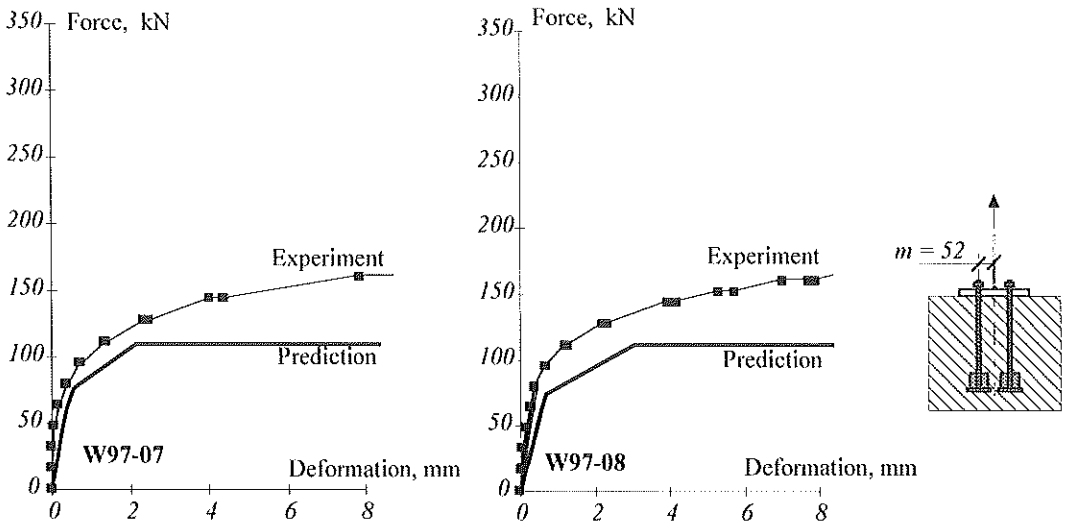

Fig 23 The load deflection diagram of experiments W97-07 and W97-08, plate thickness 12 mm

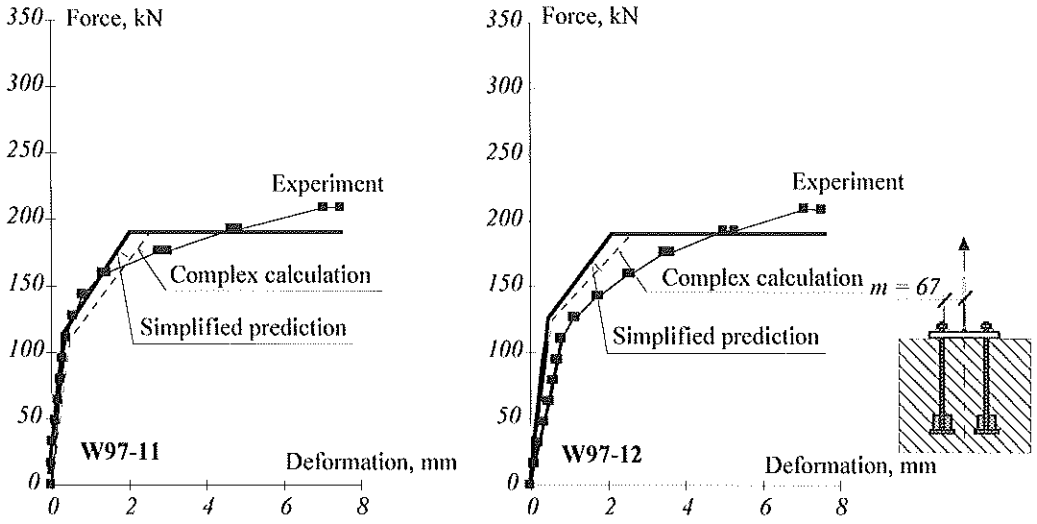

Figure 24 The load deflection diagram of experiments W97-11 and W97-12, plate thickness 20 mm

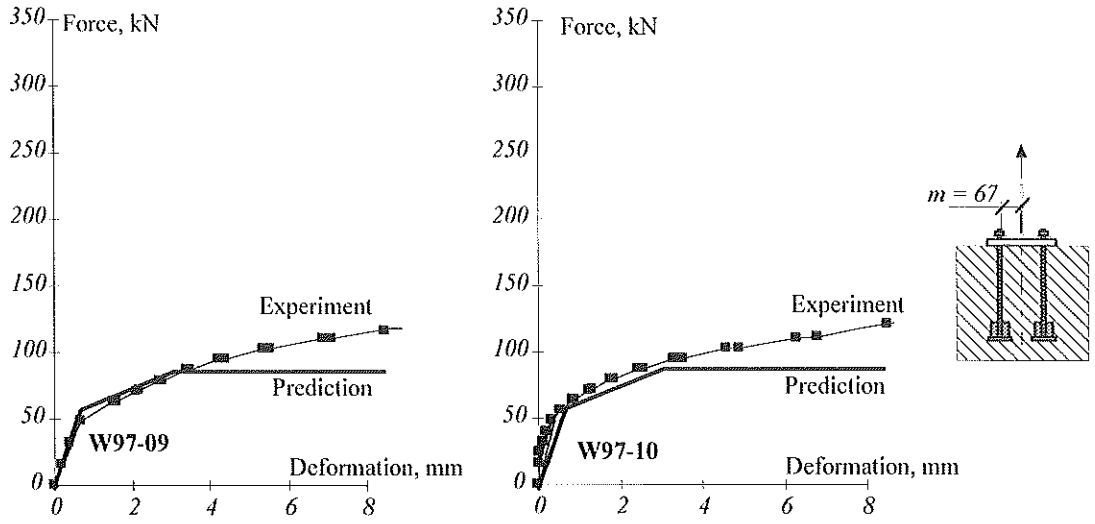

Figure 25 The load deflection diagram of experiment W97-09 and W97-10, plate thickness 12 mm